

Joint Rate Control and Demand Balancing for Electric Vehicle Charging

Fanxin Kong¹, Xue Liu², Insup Lee¹

¹University of Pennsylvania, ²McGill University

Abstract—Charging stations have become indispensable infrastructure to support the rapid proliferation of electric vehicles (EVs). The operational scheme of charging stations is crucial to satisfy the stability of the power grid and the quality of service (QoS) to EV users. Most existing schemes target either of the two major operations: charging rate control and demand balancing. This partial focus overlooks the coupling relation between the two operations and thus causes the degradation on the grid stability or customer QoS. A thoughtful scheme should manage both operations together. A big challenge to design such a scheme is the aggregated uncertainty caused by their coupling relation. This uncertainty accumulates from three aspects: the renewable generators co-located with charging stations, the power load of other (or non-EV) consumers, and the charging demand arriving in the future. To handle this aggregated uncertainty, we propose a stochastic optimization based operational scheme. The scheme jointly manages charging rate control and demand balancing to satisfy both the grid stability and user QoS. Further, our scheme consists of two algorithms that we design for managing the two operations respectively. An appealing feature of our algorithms is that they have robust performance guarantees in terms of the prediction errors on these three aspects. Simulation results demonstrate the efficacy of the proposed operational scheme and also validate our theoretical results.

I. INTRODUCTION

With the advancements in connectivity of physical devices, we are researching the era of Internet of Things (IoT). IoT allows more direct integration of the physical world into cyber systems, and thus enables various new services and applications such as vehicular communication and smart grids. This paper studies an application, smart electric vehicle (EVs) charging, which is built on the support of vehicle-to-infrastructure communication and smart grid technologies.

The market share of EVs keeps proliferating due to the benefits of few emissions and high power efficiency. As stated by the market research reports such as [1], [2], the yearly EV sales for U.S. have grown more than 6 times since 2010 and electric vehicles would hold about 28% of the U.S. vehicle market by 2031. The increasing integration of EVs introduces a high impact on the power grid by shifting the energy load from gasoline to electricity. This expected impact has drawn great interests from both the industry and academia. Thus, various charging facilities have been studied, such as charging points in residential areas and those at workplaces [3]–[5]. Among them, charging stations have become indispensable infrastructure to support the deep penetration of EVs [6], [7]. To guarantee both the stability of the power grid and the quality of service (QoS) to EV users, the operational scheme of charging stations needs careful designing.

Charging rate control and demand balancing are two major operations in a charging system with multiple charging stations. The former operation controls charging rates (or charging power) of EVs at charging stations and the latter operation balances charging demand among multiple stations.

The two operations are coupled via power provisioning. Charging stations with larger provisioned power can serve more EVs and thus more demand should be scheduled to them. On the other hand, serving more charging demand may lower the charging rates of EVs at the stations. However, most existing works study the two operations separately and focus on either of charging rate control (e.g., [8]–[12]) or charging demand balancing (e.g., [13]–[15]). The most closely related work [16], which considers both operations together, however, simply overlooks the coupling relation between the two operations.

These existing works can cause significant deviation from optimizing the grid stability or user QoS. For example, schemes solely performing demand balancing would schedule much arriving demand to the charging stations with small backlog demand. Meanwhile, these stations may have lower provisioned power supply. Aggressively charging (with high power) the arriving EVs would meet the user QoS but compromise the grid stability, and vice versa. A thoughtful design for the operational scheme should consider the coupling relation and jointly manage charging rate control and demand balancing. To design and analyze such an operational scheme, however, is a non-trivial task due to several challenges.

One big challenge is the aggregated uncertainty that accumulates from the following three key aspects. This accumulation is caused by the coupling relation between charging rate control and demand balancing. First, to meet the sustainable development needs, charging stations today increasingly employ some co-located renewable energy such as solar and wind power [17]–[19]. Renewable generation is intermittent and hard to predict. Second, since charging stations usually have no ability to control the power load of other consumers (i.e., not EVs at the stations), this non-EV load is also uncertain as to the charging stations [20]. Third, it is difficult to have an accurate estimation on the charging demand that arrives in the future. It is unrealistic to assume perfectly knowing future information of the three aspects [14]. Further, the necessity to study these uncertainties is at least twofold. First, the prediction error or the uncertainty of an individual aspect may be small, but the aggregated uncertainty can be rather large. Second, it is essential to understand how these uncertainties affect the performance of an algorithm using them as input. For example, if affecting in an exponential way, a small prediction error can make the algorithm’s output far from the realistic optimum. And, if affecting in a linear way, the algorithm’s result can be accurate enough for practical deployment.

Another challenge is the trade-off between the stability of the power grid and the charging duration of EVs. Supplying higher power to EVs reduces their charging duration. This can improve QoS and better satisfy EV users, but meanwhile causes more disturbance to the grid, and vice versa. Separately targeting the grid stability and user QoS can derive an ineffec-

tive or even infeasible operational scheme. The last challenge is that EV user behavior is spontaneous and thus hardly controllable. For instance, an EV may enter any neighboring charging stations and it would be unreasonable for the station to refuse serving the EV. Thus, it is impractical to implement a deterministic operational scheme to enforce the user behavior.

To address the above challenges, we propose a hierarchical operational scheme that jointly manages charging rate control and demand balancing in presence of the aggregated uncertainty. Our scheme has two levels. The lower level uses information exchanged between charging stations and the power grid to perform charging rate control for each charging station, which solves the trade-off between the grid stability and EV charging duration. Using the provisioned power decided by the lower level, the upper level uses information collected from EVs to carry out charging demand balancing among multiple stations, which optimizes the charging delay experienced by EV users. Due to the spontaneous user behavior, the upper level leverages an incentive based method that uses the charging price as a knob to induce desirable demand balancing. For both levels, we propose stochastic optimization based algorithms, given the estimation of the likelihood of renewable generation, non-EV power load, and arriving charging demand. These algorithms have provable robust performance guarantees in terms of the prediction errors. The robustness here means that the performance guarantees are independent on any specific distribution of the prediction errors. To be specific, our main contributions are summarized as follows.

- We study both charging rate control and demand balancing and especially address their coupling relation. We propose a hierarchical operational scheme that jointly manages the two operations in presence of the aggregated uncertainty.
- We design stochastic optimization based algorithms for both charging rate control and demand balancing. We prove that our algorithms have provable robust performance guarantees. Simulation results demonstrate the efficacy of our algorithms and also validate our theoretical results.

The rest of the paper is organized as follows. Section II focuses on the lower level. Section III targets the upper level. Section IV evaluates the proposed scheme. Section V investigates the related work. Section VI concludes the paper.

II. THE LOWER LEVEL: CHARGING RATE CONTROL

As depicted in Fig. 1, our operational scheme for a charging system has two levels. In the lower level, each charging station has a local controller to adjust charging rates of EVs within the station. In the upper level, the charging system has a global scheduler that decides how to balance charging demand for the whole system. This section focuses on the lower level and the next section targets the upper level.

A. System Model and Problem Formulation

We consider a discrete-time model, where the control horizon is partitioned into a sequence of time slots of equal length. In practice, the time slot length could be several minutes, e.g., 5 minutes [9], [16]. In the beginning of each time slot, the

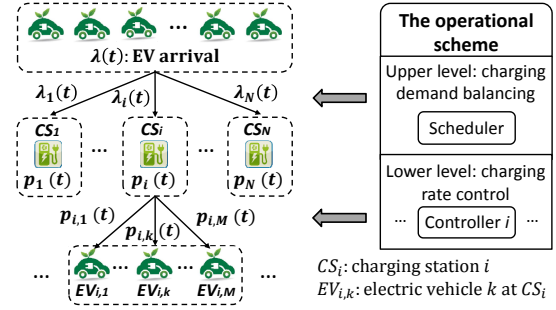


Fig. 1. The lower level is charging rate control: to adjust rate $p_{i,k}(t)$ for each EV_k at charging station CS_i . The upper level is charging demand balancing: to determine demand $\lambda_i(t)$ for each station CS_i .

controller adjusts the charging rates of all EVs at the station. We consider a single interval for the following algorithm design and analysis. The whole control process is decoupled into running the designed algorithm at every time slot. We thus omit the time index in rest of this section. That is, the following parameters are defined for a single time slot and their values could be different between different slots. This discrete-time model has been widely used in the EV charging studies such as [8], [9], [11] and power market literature such as [21]–[23]. In the rest of this section, we consider one single station and thus also omit the indices for stations.

Power supply model. Besides sourcing from the power grid, charging stations nowadays increasingly employ some local renewable energy (e.g., solar power and wind power) to meet the sustainable development needs [19]. We thus consider both of these two energy sources: the power grid and co-located renewable generation. The grid feeds a charging station through a transformer. We use L to denote the nameplate capacity of the feeding transformer, which is the registered amount of power load that the transformer can serve. The following design and analysis can be easily adapted to the case where a transformer serves multiple charging stations.

The effective power output of renewable (e.g., such as solar and wind power) is uncontrollable and is usually dependent on external conditions such as solar irradiation and wind speed [24], [25]. Its fluctuation and variability bring significant difficulty in the charging control. To model this uncertainty, we use \tilde{R} to denote the predicted renewable generation and R to denote the actual renewable power output, and further $R = (1 + \varepsilon_r)\tilde{R}$, where ε_r is the prediction error. We assume that the prediction error has a mean $\mathbb{E}[\varepsilon_r] = 0$ and a variance $\mathbb{V}[\varepsilon_r] = \sigma_r^2$, which can be obtained using historic data. These assumptions are standard in statistics [25], [26].

Power load model. The power load on the feeding transformer can be differentiated into two different types: inelastic base load of other consumers (or non-EV load) and elastic EV load of the charging station [8], [9], [11]. The elasticity here is based on whether the load can be controlled by the station.

The charging station cannot control the base load and thus stochastic modeling is used to model the base load. We use \tilde{D} to denote the predicted base load and D to denote the actual base load, and further $D = (1 + \varepsilon_d)\tilde{D}$, where ε_d is the prediction error. We assume the prediction error has a mean

$\mathbb{E}[\varepsilon_d] = 0$ and a variance $\mathbb{V}[\varepsilon_d] = \sigma_d^2$, which can be obtained from historic data. The prediction errors ε_r (for the renewable generation) and ε_d (for the base load) are independent and with finite second moments. Similarly, these assumptions are standard in statistics [25], [26]. Discussing the approaches for predicting renewable or base load is out of scope of this paper. Interested readers may refer to works such as [24], [27].

The station is charging M EVs, and each of them has a rate p_k . The EV load p equals the sum of rates of all M EVs, i.e., $p = \sum_k p_k$. In this level, each EV is characterized by two parameters: a charging rate limit and a disutility function. First, EVs have charging rate limits (or maximum rates) and different types of EVs support different limits. For example, Nissan Leaf is able to support $50kW$ while Tesla Model S can support up to $120kW$ [28]. Thus, without loss of generality, we assume that each EV_k has a different charging rate limit, denoted by \bar{P}_k . Second, a disutility function is used to quantify the utility loss that EV_k takes when it has a charging rate of p_k . Since large rate results in short charging duration, the disutility can be seen as how much the EV user is dissatisfied with charging rate p_k with respect to the charging duration. Further, according to EV charging studies such as [10], [11], EV users may have different degrees of satisfaction even though their EVs have the same charging rate. Two possible reasons are their different state of charge and different battery capacity. We use a weight $\alpha_k > 0$ to capture this heterogeneity among EVs and attribute each EV_k with a disutility $U(\alpha_k, p_k)$. The weight is constant within a time slot and may be different between different slots. We assume the disutility function is continuously differentiable, non-increasing and strictly concave as to p_k . The disutility equals zero when charging at the maximum rate \bar{P}_k and is maximal when charging no power. Though this kind of modeling may seem restrictive, it is standard and has been widely used within the power markets literature such as [8], [21]–[23], [29], [30]. Note that the following analysis will be similar if we define a utility function with properties of continuous differentiability, non-decrease and strict concavity.

A transformer usually can operate lightly overloaded, which however will cause its temperature rise and thus compromise both its reliability (thus affect the grid stability) and lifetime [31], [32]. For the feeding transformer, we use a penalty function $S(\cdot)$ to capture the penalty on the amount that the feeding transformer is overloaded with. In addition, when the renewable generation is surplus as to the EV load, it can be used for the base load. This brings mutual benefits for the power grid and the charging station. For example, by sharing the renewable, the power load on the feeding transformer can be reduced, and thus its reliability increases and provides more reliable power to the charging station; besides having more reliable power supply, the charging station may also obtain some revenue from sharing the renewable. This kind of sharing energy generation has been brought up as the major function of microgrids, which is regarded as a major vision of the smart grid [33], [34]. Thus, the overload on the feeding transformer is $[p + D - R - L]^+$ and the penalty is $S([p + D - R - L]^+)$,

where $[a]^+ = \max\{0, a\}$. We assume that this penalty function $S(\cdot)$ is convex and non-negative, and has a global minimum $S(0) = 0$, and is continuously differentiable with $S'(0) = 0$. As mentioned above, this kind of modeling has been widely used within the power markets literature.

Problem formulation. We use a notion of social cost defined as the sum of EVs's disutility and the penalty associated with the feeding transformer. The goal of the charging control problem is to minimize the social cost, and the problem can be formulated as the following optimization problem:

$$\min \quad u(\mathbf{p}) = \sum_k U(\alpha_k, p_k) + S(e) \quad (1)$$

$$s.t. \quad e = [p + D - R - L]^+, \quad (2)$$

$$p = \sum_k p_k, \quad (3)$$

$$0 \leq p_k \leq \bar{P}_k, \quad \forall k, \quad (4)$$

where $\mathbf{p} = (p_k)_{\forall k}$ is the vector of charging rates. The objective Eqn. (1) is to minimize the social cost. Eqn. (2) defines how much the feeding transformer is overloaded. Eqn. (3) is the sum of charging rates of all EVs in the charging station. Eqn. (4) limits the charging rate of each EV.

B. Expected Social Cost Optimization

In this subsection, our goal is to control the charging rate in order to minimize the expected social cost given the estimations of the renewable generation and base load. The corresponding optimization problem based on the predictions becomes to Eqn. (1), Eqn. (3), Eqn. (4), and $e = [p + \tilde{D} - \tilde{R} - L]^+$, where \tilde{D} and \tilde{R} are the predicted base load and renewable generation respectively. We use \mathbf{P}_1^e to denote this problem and our algorithm solves this problem. To analyze the performance of our algorithm, we assume an oracle-like off-line algorithm that perfectly knows the actual renewable generation and based load. The off-line algorithm solves the problem given by Eqn. (1)(2)(3)(4), which is denoted by \mathbf{P}_1^o . The optimal solution of problem \mathbf{P}_1^e is denoted as $\tilde{\mathbf{p}} = (\tilde{p}_k)_{\forall k}$ and let $\tilde{p} = \sum_k \tilde{p}_k$. The resulting social cost is thus

$$u(\tilde{\mathbf{p}}) = \sum_k U(\alpha_k, \tilde{p}_k) + S(\tilde{e}), \quad (5)$$

where $\tilde{e} = [\tilde{p} + D - R - L]^+$. Since the control decisions are made at the beginning of each time slot, we use the solution $\tilde{\mathbf{p}}$ to calculate the social cost in Eqn. (5). By contrast, the penalty on the feeding transformer depends on the actual renewable generation and base load, and thus we use the actual value R and D to calculate the penalty $S(\hat{e})$ in Eqn. (5). Similarly, the optimal solution of problem \mathbf{P}_1^o is denoted as $\hat{\mathbf{p}} = (\hat{p}_k)_{\forall k}$ and let $\hat{p} = \sum_k \hat{p}_k$. The resulting social cost is thus

$$u(\hat{\mathbf{p}}) = \sum_k U(\alpha_k, \hat{p}_k) + S(\hat{e}), \quad (6)$$

where $\hat{e} = [\hat{p} + D - R - L]^+$.

The performance of \mathbf{P}_1^e is dependent on the accuracy of the predictions on renewable generation and base load. We now characterize this dependence. To analyze the performance of \mathbf{P}_1^e , we use the competitive ratio, which is defined as the ratio of the social cost of a given algorithm to that of the off-line

optimal algorithm. Here, it is denoted as $\eta_l = \frac{\mathbb{E}[u(\hat{\mathbf{p}})]}{\mathbb{E}[u(\bar{\mathbf{p}})]}$, given Eqn. (5) and Eqn. (6). Before evaluating the competitive ratio, we give a lemma, which will be used in the following proofs.

Lemma 1: The optimal solution of the optimization problem given by Eqn. (1)(2)(3)(4) remains the same if replacing Eqn. (2) with $e = p + D - R - L$.

Proof: We use the definition of the disutility and the penalty function to prove this lemma. We call the original problem as P1 and the new one (with the replaced constraint) as P2. It is easy to know that P1 is equivalent to P2 when $e \geq 0$. When $e < 0$, the feeding transformer has load less than L . The objective of P1 becomes to $\sum_k U(\alpha_k, p_k)$ because $S(0) = 0$. The objective is decreasing with respect to $p_k, \forall k$. On the other hand, since $S'(0) = 0$, $S(e)$ is decreasing with respect to $e < 0$ and thus it is decreasing as to $p_k, \forall k$. The objective of P2 is also decreasing as to $p_k, \forall k$. Hence, both problems achieve the optimum when $p_k = \bar{P}_k, \forall k$. ■

The problems P1 and P2 in the proof only have the same resulting charging rates, but the optimal social cost may be different. Further, this lemma allows an easier way to solve problem P1. That is, we first solve problem P2, and then insert the resulting charging rates into the original problem P1 to obtain its optimal social cost. Thus, the lemma provides a key property that facilitates the following competitive analysis.

Evaluating the competitive ratio η_l . To explicitly evaluate the competitive ratio, we need restrict disutility $U(\cdot)$ and penalty $S(\cdot)$ to some specific forms. We use the following two specific functions for the disutility and penalty:

$$U(\alpha_k, p_k) = \frac{1}{2} \alpha_k (\bar{P}_k - p_k)^2, \forall k, \text{ and } S(e) = \frac{1}{2} e^2. \quad (7)$$

This may seem restrictive, but these two functions have been widely used with the power market literatures such as in [21]–[23], [29], [30]. We then can explicitly compute the optimal charging rates for problem \mathbf{P}_1^e and \mathbf{P}_1^o as shown by Eqn. (8) and Eqn. (9), respectively. Lemma 2 shows the relation between \tilde{p}_k and \hat{p}_k . Let $\Psi_k = (\alpha_k(1 + \sum_k \frac{1}{\alpha_k}))^{-1}$, we have

$$\tilde{p}_k = \left[\bar{P}_k - \tilde{\beta}_k \right]_0^{\bar{P}_k}, \text{ where } \tilde{\beta}_k = \Psi_k (\sum_k \bar{P}_k + \tilde{D} - \tilde{R} - L), \quad (8)$$

$$\hat{p}_k = \left[\bar{P}_k - \hat{\beta}_k \right]_0^{\bar{P}_k}, \text{ where } \hat{\beta}_k = \Psi_k (\sum_k \bar{P}_k + D - R - L), \quad (9)$$

where $[x]_b^a = \min\{\max\{x, b\}, a\}$, which projects x into the range of $[b, a]$. Eqn. (8) (Eqn. (9)) is derived by first calculating the stationary point of Eqn. (5) (Eqn. (6)), and then projecting the point, i.e., $\bar{P}_k - \tilde{\beta}_k$ (i.e., $\bar{P}_k - \hat{\beta}_k$), into the charging rate range $[0, \bar{P}_k]$. It is easy to know that Eqn. (8) (Eqn. (9)) is the optimal solution for problem \mathbf{P}_1^e (problem \mathbf{P}_1^o) [35].

Lemma 2: The optimal solutions of problem \mathbf{P}_1^e and \mathbf{P}_1^o satisfy $\tilde{p}_k = \hat{p}_k + \varphi_k$ and $\varphi_k = \varphi_k^+ + \varphi_k^-$, where

$$\begin{aligned} \varphi_k^+ &= \left[\varepsilon_k + \tilde{\beta}_k \right]_0^{\varepsilon_k^+} - \left[\bar{P}_k - \tilde{\beta}_k \right]_{\varepsilon_k^-}^0, \\ \varphi_k^- &= \left[-\tilde{\beta}_k \right]_{\varepsilon_k^-}^0 - \left[\varepsilon_k - \bar{P}_k + \tilde{\beta}_k \right]_0^{\varepsilon_k^+}, \\ \text{where } \varepsilon_k &= \Psi_k (\varepsilon_d \tilde{D} - \varepsilon_r \tilde{R}). \end{aligned} \quad (10)$$

Proof: For better readability, we put all proofs of all lemmas and theorems in Appendix. ■

We further give a lemma that bounds the expectations $\mathbb{E}[\varepsilon_r^+ - \varepsilon_r^-]$, $\mathbb{E}[\varepsilon_d^+ - \varepsilon_d^-]$, and variances $\mathbb{V}(\varepsilon_r^+ - \varepsilon_r^-)$, $\mathbb{V}(\varepsilon_d^+ - \varepsilon_d^-)$, which will be used when proving the competitive ratio.

Lemma 3: The prediction error ε_r has a property that $E[\varepsilon_r^+ - \varepsilon_r^-] \leq \sigma_r$, $\mathbb{V}(\varepsilon_r^+ - \varepsilon_r^-) \leq \sigma_r^2$, and the prediction error ε_d has a property that $E[\varepsilon_d^+ - \varepsilon_d^-] \leq \sigma_d$, $\mathbb{V}(\varepsilon_d^+ - \varepsilon_d^-) \leq \sigma_d^2$.

We now give the main theorem of this section as follows. The theorem bounds the competitive ratio and demonstrates that the social cost of \mathbf{P}_1^e is close to the optimal value of \mathbf{P}_1^o if the predictions are accurate.

Theorem 4: Given that the variance of prediction errors of the renewable generation and base load are σ_r^2 and σ_d^2 , solving problem \mathbf{P}_1^e has a competitive ratio of

$$\eta_l \leq 1 + A_1 \left(\tilde{D}^2 \sigma_d^2 + \tilde{R}^2 \sigma_r^2 + \tilde{D} \sigma_d \tilde{R} \sigma_r \right) + A_2 \left(\tilde{D} \sigma_d + \tilde{R} \sigma_r \right),$$

where A_1 and A_2 are given by Eqn. (11).

$$\begin{aligned} A_1 &= \frac{\sum_k \alpha_k \Psi_k^2 + (\sum_k \Psi_k)^2}{\mathbb{E}[u(\hat{\mathbf{p}})]}, \\ A_2 &= \frac{\sum_k \alpha_k (\bar{P}_k - \hat{p}_k) \Psi_k + \hat{e} \sum_k \Psi_k}{\mathbb{E}[u(\hat{\mathbf{p}})]}. \end{aligned} \quad (11)$$

Theorem 4 does not rely on any assumptions on the distribution of the prediction errors (for both the renewable generation and base load) other than the bounded variance. The competitive ratio is a linear function of the variance and standard deviation of the prediction errors. It decreases to 1 (i.e., our algorithm derives the realistic optimum), when the prediction errors decrease to 0. Thus, our algorithm based on problem \mathbf{P}_1^e is fairly robust to the prediction errors.

III. THE UPPER LEVEL: CHARGING DEMAND BALANCING

The upper level studies how to balance charging demand among multiple stations for the whole system. We consider a charging system that has multiple charging stations in an urban area. As illustrated in Fig. 1, the scheduler of the system carries out charging demand balancing. One thread of related work assumes that the behavior of EV users is controllable and design deterministic demand balancing algorithms for the scheduler, such as [7], [15]. These algorithms are plausible if EV users will exactly follow the scheduling decisions. However, in reality, EV user behavior is spontaneous and thus hardly controllable. For example, an EV may enter any neighboring charging stations, and it is hard for the station to refuse serving the EV user or force her to other stations. Further, to ensure privacy, EV users may not want to give their charging information to charging stations before they make decisions. Thus, the deterministic approaches may even not be feasible in reality due to lack of the charging information. To address these two issues, we study the uncertainty of the user behavior and employ an incentive-based method. Specially, the designed scheduler leverages the charging price as a knob to induce desirable demand balancing. The price is dynamically set according to both the arriving charging demand and demand backlog at charging stations.

A. System Model and Problem Formulation

We also employ a discrete-time model here and the schedule horizon is partitioned into a sequence of time slots of equal duration. The time slot length is equal to that defined in the previous section. In each time slot, there are two kinds of operations: rate control and demand balancing. That is, the controller first adjusts charging rates of EVs in each station and then the scheduler balances charging demand of the whole system. Charging rate control for each station is already studied in the previous section. Thus, we focus on designing demand balancing algorithms for whole system in this section. We consider a single time slot for the following algorithm design. The whole schedule process is decoupled into running the designed algorithm at every time slot.

Queueing model for multiple stations. We consider an urban area, where N stations exist in the neighborhood of EVs. These stations are modeled as a multi-queue system with N queues, and each station corresponds to one queue. We denote $Q_i(t)$ as the queue size or the demand backlog of station CS_i at the beginning of time slot t . Their dynamics are

$$Q_i(t+1) = [Q_i(t) - \mu_i(t)]^+ + \lambda_i(t), \forall i, \quad (12)$$

where $\mu_i(t)$ and $\lambda_i(t)$ are described as follows. The parameter $\mu_i(t)$ is the total charging rate of all EVs at station CS_i during time slot t . It is determined by the rate control algorithms in Section II and reflects the coupling relation between the two levels. We use $\tilde{\mu}_i(t)$ to denote the total charging rate decided by our charging rate control algorithm (solving problem \mathbf{P}_1^e), and thus $\tilde{\mu}_i(t) = \sum_k \tilde{\mu}_k(t)$. We further use $\hat{\mu}_i(t)$ to denote the total charging rate by the off-line optimal algorithm (solving problem \mathbf{P}_1^o), and thus $\hat{\mu}_i(t) = \sum_k \hat{\mu}_k(t)$. The parameter $\lambda_i(t)$ denotes the charging demand of station CS_i during time slot t . To balance charging demand is to determine $\lambda_i(t)$ for each charging station CS_i . We see that the backlog of charging demand of charging station CS_i represents the charging delay experienced by EV users. The more backlog a station has, the larger delay EV users will experience. We use a disutility function $G(Q_i(t))$ to capture the QoS degradation caused by the demand backlog. The function $G(Q_i(t))$ is assumed to be convex and non-negative, and has a global minimum $G(0) = 0$, and is continuously differentiable with $G'(0) = 0$. This kind of modeling has been widely used within the queueing network and EV charging studies such as [13], [36], [37].

We use $\lambda(t)$ to denote the total actual arriving charging demand of the whole system during time slot t . This actual demand $\lambda(t)$ is known at the end of slot t . However, to perform demand balancing, the scheduler needs to know the demand $\lambda(t)$ at the beginning of time slot t . Thus, at this time, the scheduler first makes a prediction on $\lambda(t)$. Based on the prediction, the scheduler then carries out demand balancing. We use $\tilde{\lambda}(t)$ to denote the predicted total demand and let $\lambda(t) = (1 + \varepsilon_\lambda)\tilde{\lambda}(t)$, where ε_λ is the prediction error. We assume that the prediction error ε_λ has a mean $\mathbb{E}[\varepsilon_\lambda] = 0$ and a variance $\mathbb{V}[\varepsilon_\lambda] = \sigma_\lambda$. The prediction error ε_λ has a finite second moment and is independent of ε_r and ε_d (the prediction

errors of renewable and based load defined in Section II). These assumptions are standard in statistics [25], [26].

Demand response model for charging demand. As mentioned, the behavior of EV users is hardly controllable. Thus, we use charging price as an incentive to induce a balanced allocation of charging demand. We use $q_i(t)$ to denote the charging price for the charging demand $\lambda_i(t)$ of charging station CS_i during time slot t . In order not to affect the EVs being charging at a station, the charging price is fixed for an EV after it arrives at the station. We assume that all EV users have the same demand response preference on choosing stations. First, since we consider an urban area and all EVs are in the neighborhood of charging stations, we assume that distance between EVs and charging stations has little effect on users' preference. So we see the charging price as the dominant factor when EV users making decisions. They prefer lower charging price to higher charging price. Second, all charging stations may be overloaded or have much backlog sometime. To reduce the backlog or the potential charging delay, all stations set very high charging prices and induce users not to choose them. Seeing all high price, EV users may choose none of them, and give up charging at the time and search for charging at later time. Thus, we assume that EV users are only concerned about the absolute charging price instead of relative price between different stations. These are common settings on users' preference in EV charging studies such as [13], [14], [38]. We use a function $f(q_i(t))$ to denote the probability of choosing station CS_i when the station sets its charging price as $q_i(t)$. Thus, the probability of not choosing station CS_i is $1 - f(q_i(t))$. The probability function $f(q_i(t))$ is non-negative and is continuously differentiable, non-increasing and concave with respect to charging price $q_i(t)$. Other dimensions, such as geographical proximity to stations, daytime and nighttime, can also affect the probability. We consider these dimensions as constant factors as to the probability when charging stations make one decision at a time. That is, stations can only adjust their charging prices to affect the probability, not these dimensions. Hence, we only focus on the dimension of price in the probability function in this paper. The applicability of this demand response modeling method has been verified in EV charging works such as [13], [14].

Problem formulation. We use a notion of social cost defined as the sum of charging cost and the disutility of charging demand associated with each station. The social cost definition here is different from that defined in Section II. The goal of charging demand balancing is to minimize the social cost, and it can be formulated as:

$$\min \quad c(\mathbf{q}(t)) = \sum_i q_i(t)\lambda_i(t) + \sum_i G(Q_i(t+1)), \quad (13)$$

$$s.t. \quad q \leq q_i(t) \leq \bar{q}, \forall i, \quad (14)$$

$$\lambda_i(t) = f(q_i(t))\lambda(t), \forall i, \quad (15)$$

$$Q_i(t+1) = [Q_i(t) - \mu_i(t)]^+ + \lambda_i(t), \forall i, \quad (16)$$

where $\mathbf{q}(t) = (q_i(t))_{\forall i}$ is the vector of charging price; $Q_i(t+1)$ is the backlog by the end of time slot t ; q and \bar{q} are the lower and upper bound of charging price. The objective

Eqn. (13) is the social cost minimization, where the first item is the total charging cost and the second item is the total disutility of all charging stations. Eqn. (14) limits the charging price of each station. Eqn. (15) is for the expected charging demand of each station. As to Eqn. (16), $\mu_i(t)$ is determined by the charging rate control in Section II. If $\mu_i(t)$ is decided by our algorithm (solving problem \mathbf{P}_i^e), it inherits uncertainty from that of renewable and base load. So there are in total three aspects, i.e., renewable, base load and demand $\lambda(t)$, that cause uncertainty. Although the above optimization problem can be decoupled into subproblems for each station, it is still difficult to carry out performance analysis due to the aggregated uncertainty. To solve this difficulty, we now present our stochastic optimization based algorithm and analyze its performance in the context of this aggregated uncertainty.

B. Expected Social Cost Optimization

In this subsection, our goal is to minimize the expected social cost through adjusting the charging price, given the charging rate $\mu_i(t)$ and the estimation on the charging demand $\lambda(t)$. We use \mathbf{P}_u^e to denote the optimization problem based on the predictions of the three aspects. To be specific, problem \mathbf{P}_u^e uses the same objective as Eqn. (13) and the same constraint as Eqn. (14). It replaces $\lambda(t)$ with $\hat{\lambda}(t)$ in the constraint Eqn. (15), and changes $\mu_i(t)$ to $\hat{\mu}_i(t)$ in the constraint Eqn. (16). Our algorithm solves problem \mathbf{P}_u^e . On the other hand, we assume an oracle-like off-line algorithm that perfectly knows the actual renewable generation, based load and charging demand $\lambda(t)$. The corresponding optimization problem, denoted as \mathbf{P}_u^o , employs Eqn. (13)(14)(15) and replaces $\mu_i(t)$ with $\hat{\mu}_i(t)$ in Eqn. (16). This off-line algorithm solves problem \mathbf{P}_u^o .

We use $\tilde{\mathbf{q}}(t) = (\tilde{q}_i(t))_{\forall i}$ to denote the optimal solution of problem \mathbf{P}_u^e . The resulting social cost is

$$c(\tilde{\mathbf{q}}(t)) = \sum_i \tilde{q}_i(t) f(\tilde{q}_i(t)) \lambda(t) + \sum_i G(\tilde{Q}_i(t+1)),$$

$$\text{where } \tilde{Q}_i(t+1) = [Q_i(t) - \tilde{\mu}_i(t)]^+ + f(\tilde{q}_i(t)) \lambda(t). \quad (17)$$

At the beginning of time slot t , the scheduling decisions are made and $\tilde{\mathbf{q}}(t)$ is decided as the charging price for the time slot. Thus, $\tilde{\mathbf{q}}(t)$ is used to calculate the probability for selecting the charging station. The social cost depends on the actual charging demand, not on the predicted value. Thus, in Eqn. (17), we use the actual value $\lambda(t)$ to calculate the social cost $c(\tilde{\mathbf{q}}(t))$. Similarly, we use $\hat{\mathbf{q}}(t) = (\hat{q}_i(t))_{\forall i}$ to denote the optimal solution of problem \mathbf{P}_u^o . The resulting social cost is

$$c(\hat{\mathbf{q}}(t)) = \sum_i \hat{q}_i(t) f(\hat{q}_i(t)) \lambda(t) + \sum_i G(\hat{Q}_i(t+1)),$$

$$\text{where } \hat{Q}_i(t+1) = [Q_i(t) - \hat{\mu}_i(t)]^+ + f(\hat{q}_i(t)) \lambda(t). \quad (18)$$

The performance of \mathbf{P}_u^e depends on the accuracy of the prediction on demand $\lambda(t)$ as well as that on renewable and base load (through $\tilde{\mu}_i(t), \forall i$). We now characterize this dependence and also use competitive analysis to analyze the performance of \mathbf{P}_u^e . The competitive ratio in this section is denoted as $\eta_u = \frac{\mathbb{E}[c(\tilde{\mathbf{q}}(t))]}{\mathbb{E}[c(\hat{\mathbf{q}}(t))]}$, given Eqn. (17) and Eqn. (18).

Evaluating the competitive ratio η_u . To explicitly evaluate the competitive ratio, we need to restrict the charging station

selection probability $f(\cdot)$ and disutility $G(\cdot)$ to some specific forms. We adopt the following two specific functions for the probability and disutility respectively:

$$f(q_i(t)) = \frac{1}{\Delta q} (\bar{q} - q_i(t)), \quad \forall i, \text{ where } \Delta q = \bar{q} - \underline{q}, \quad (19)$$

$$\text{and } G(Q_i(t)) = \omega Q_i^2(t), \quad (20)$$

where ω is the weight between the charging cost and the disutility. The linear probability function Eqn. (19) is proposed in [39], and thereafter, it has been widely used to model customer behavior (including EV user behavior, e.g. [13]). The disutility function Eqn. (20) is classic as to the queueing network literature (e.g., [36]). The optimal charging prices for problem \mathbf{P}_u^e and \mathbf{P}_u^o are

$$\tilde{q}_i(t) = \left[\bar{q} + \tilde{\theta}_i \right]_{\underline{q}}^{\bar{q}}, \quad \text{where } \tilde{\theta}_i = \Delta q \frac{2\omega [Q_i(t) - \tilde{\mu}_i(t)]^+ + \bar{q}}{2\omega \lambda(t) - 2\Delta q}, \quad (21)$$

$$\hat{q}_i(t) = \left[\bar{q} + \hat{\theta}_i \right]_{\underline{q}}^{\bar{q}}, \quad \text{where } \hat{\theta}_i = \Delta q \frac{2\omega [Q_i(t) - \hat{\mu}_i(t)]^+ + \bar{q}}{2\omega \lambda(t) - 2\Delta q}. \quad (22)$$

Eqn. (21) (Eqn. (22)) is derived by projecting the stationary point of Eqn. (17) (Eqn. (18)) into the price rate range $[q, \bar{q}]$. They are the optimal solutions for problem \mathbf{P}_u^e and \mathbf{P}_u^o [35].

To better induce EV users and better balance charging demand, a charging system should have a wide and well defined price range. If the charging system gives no such consideration, the price can be the boundary values \bar{q} and \underline{q} at most time. It is trivial to bound difference between \tilde{q} and \hat{q} , which is $[-\Delta q, \Delta q]$. This much eases the competitive analysis. By contrast, we focus on a well defined price range and provide the competitive analysis for the non-trivial case. Thus, we use a well-defined price range that needs no projection into the range, i.e., the solution inner $[\cdot]$ naturally lies in $[q, \bar{q}]$. To make the inner part less than \bar{q} naturally, we have

$$\bar{q} - \underline{q} > \omega \max_t \lambda(t), \quad (23)$$

and to make it greater than \underline{q} naturally, we have

$$\bar{q} - 2\underline{q} \geq 2\omega [\max_{i,t} Q_i(t) - \min_{i,t} \mu_i(t)]^+ + 2\omega \max_t \lambda(t), \quad (24)$$

where $\max_t \lambda(t)$, $\max_{i,t} Q_i(t)$, and $\min_{i,t} \mu_i(t)$ can be obtained using historical data. Thus, the well defined price range needs to satisfy: $\bar{q} > \underline{q} > 0$ and Eqn. (24). In the following analysis, we let $\tilde{q}_i(t)$ and $\hat{q}_i(t)$ be the inner parts of $[\cdot]_{\underline{q}}^{\bar{q}}$ in Eqn. (21) and Eqn. (22), respectively. We consider one single time slot and omit the time index. We now give the main theorem of this section, which bounds the competitive ratio. The theorem demonstrates the social cost of \mathbf{P}_u^e is close to the optimal (by \mathbf{P}_u^o) if the predictions are accurate.

Theorem 5: Given that the variance of prediction errors of the arriving charging demand, renewable and base load are σ_λ^2 , σ_r^2 , and σ_d^2 , solving problem \mathbf{P}_u^e has a competitive ratio of

$$\eta_u \leq 1 + \sum_i \left(B_{1,i} \sigma_\lambda + B_{2,i} \left(\tilde{D}_i^2 \sigma_d^2 + \tilde{R}_i^2 \sigma_r^2 + \tilde{D}_i \sigma_d \tilde{R}_i \sigma_r \right) + B_{3,i} \left(\tilde{D}_i \sigma_d + \tilde{R}_i \sigma_r \right) \right), \quad (25)$$

where $B_{1,i}$, $B_{2,i}$ and $B_{3,i}$ are given by Eqn. (26), Eqn. (27) and Eqn. (28), respectively.

TABLE I

THE PARAMETER SETTING FOR THREE CHARGING STATIONS. RENEWABLE GENERATION AND BASE LOAD ARE THEIR ACTUAL VALUES.

	CS_1	CS_2	CS_3
No. of EVs (K_i)	10	15	20
Backlog (Q_i) (MWh)	0.05	0.1	0.15
Base load (D_i) (MW)	1.8	2	2.5
Transformer (L_i) (MW)	2	2.5	3
Renewable (R_i) (MW)	0.2	0.25	0.3

$$B_{1,i} = \frac{1}{\mathbb{E}[c(\bar{q})]} \frac{\omega\lambda\bar{\lambda}(4\Delta q - 3\omega\bar{\lambda} - \omega\lambda)}{2(\Delta q - \omega\lambda)(\Delta q - \omega\bar{\lambda})^2} \left(\frac{\bar{q}}{2} + \omega[Q_i - \hat{\mu}_i]^+ \right)^2, \quad (26)$$

$$B_{2,i} = \frac{1}{\mathbb{E}[c(\bar{q})]} \frac{2\omega(\Delta q + 2\omega\lambda - \omega\bar{\lambda})}{\Delta q - \omega\bar{\lambda}} \left(\sum_k \Psi_{i,k} \right)^2, \quad (27)$$

$$B_{3,i} = \frac{1}{\mathbb{E}[c(\bar{q})]} \left(\frac{\omega\lambda(\bar{q} + 2\omega[Q_i - \hat{\mu}_i]^+)(2\Delta q - \omega\bar{\lambda} - \omega\lambda)}{(\Delta q - \omega\bar{\lambda})^2} + \frac{\omega\lambda\bar{q}}{\Delta q - \omega\lambda} + 2\omega[Q_i - \hat{\mu}_i]^+ \right) \left(\sum_k \Psi_{i,k} \right). \quad (28)$$

Theorem 5 does not rely on any assumptions on the distribution of the prediction errors. The competitive ratio is a linear function of the variance and/or standard deviation of the prediction errors of all the three aspects (including renewable, base load, and arriving charging demand). The ratio decreases to 1 when the prediction errors decrease to 0. The algorithm solving problem \mathbf{P}_u^e is thus fairly robust to the prediction errors. These observations are similar to that for Theorem 4.

IV. EVALUATION

Until now, we have provided theoretical performance guarantees for the proposed algorithms. In this section, we evaluate these algorithms using numerical simulations to obtain a better picture of their performance.

A. Experimental Setup

We consider an urban area with three charging stations. Each station has co-located renewable and sources from the power grid through a different feeding (medium voltage) transformer. Table I shows the parameter setting for the three stations. For the whole charging system, we assume that the actual arrival demand λ is $0.15 MWh$. The charging price has the same scale with the realistic retail electricity price and its range is set as $[0.05, 0.2] \$/kWh$ [40]. The time slot length is set as 5 minutes. The weight w in Eqn. (20) is set to be 400. For each EV, its charging limit $\bar{P}_{i,k}$ is uniformly generated from a range of $[20, 120] kW$. This range has the same scale with the real EV maximum charging power, e.g., Nissan Leaf supports $50kW$ and Tesla Model S supports $120kW$ [28]. The weight $\alpha_{i,k}$ in Eqn. (7) is chosen from the uniform distribution in the range of $[200, 600]$. The above is the default parameter setting. We will also change the parameters accordingly when carrying out sensitivity analysis.

B. Experimental Results

1) *Charging Rate Control*: Fig. 2(a) to Fig. 2(c) show the performance of the proposed charging rate control algorithm as to the three charging stations, CS_1 , CS_2 and CS_3 . These figures demonstrate how the competitive ratio varies with the prediction errors. First, the competitive ratio rises as the inaccuracy of base load prediction (i.e., σ_{D_1} , σ_{D_2} and σ_{D_3})

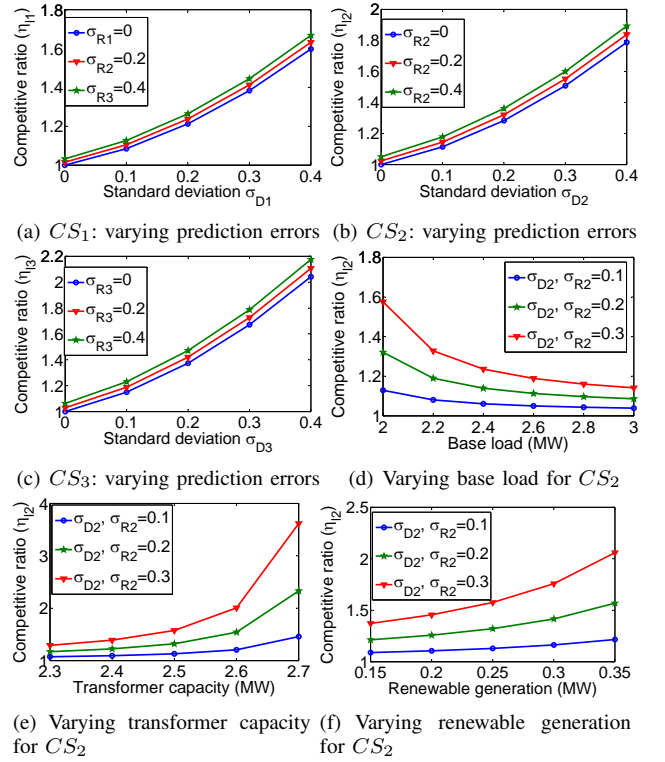


Fig. 2. Comparison on competitive ratios by varying prediction errors, backlog, base load and renewable generation.

increases. Comparing these three curves in one figure (e.g., Fig. 2(b)), we can see that the competitive ratio also increases as the inaccuracy of renewable generation prediction (i.e., σ_{R_1} , σ_{R_2} and σ_{R_3}) increases. Further, their increasing rates are super linear as to the prediction errors. These observations also validate Theorem 4. Second, the proposed algorithm gives rather good performance, even when the prediction inaccuracy is acceptable. For example, for all the three figures, when the prediction errors are less than 10% and 20%, the competitive ratios are less than 1.2 and 1.4, respectively.

One more observation from the three figures is that the prediction error on the base load (i.e., σ_{D_1} , σ_{D_2} and σ_{D_3}) has higher impact on the performance than the prediction error on the co-located renewable generation (i.e., σ_{R_1} , σ_{R_2} and σ_{R_3}) does. This can be observed from that the three curves in one figure are close to each other along the vertical axis while they are more steep along the horizontal axis. The reason for this observation is that the scale of base load is much larger than the scale of the renewable generation, which also follows the reality. Thus, even when they have the same prediction error (e.g., $\sigma_{D_2} = \sigma_{R_2}$), the inaccuracy of base load prediction causes more performance degradation. We can see that the three charging stations have similar simulation results. Thus, in the rest of this subsection, we use one charging station, i.e., CS_2 , as an example to conduct other sensitivity analysis.

Fig. 2(d) depicts how the competitive ratio varies with the base load. Each curve is plotted with fixed prediction errors of base load and renewable generation. For example, the triangle-dotted curve is when $\sigma_{D_2} = 0.1$ and $\sigma_{R_2} = 0.1$. One observation is that as the base load grows, the competitive ratio

decreases and the decreasing rate also reduces. The reason is as the following. When the base load becomes larger, the charging station draws less power from the grid because of the transformer capacity limit. Further, the uncertainty of base load affects the performance through the power drawn by the charging station from the power grid. Thus, the grid power's impact on the performance becomes smaller and the station depends more on the co-located renewable generation. On the other hand, as mentioned above, the scale of the renewable generation is small and thus has low impact on the algorithm's performance. Hence, the competitive ratio declines. At the extreme case, there is no grid power left for the charging station when the base load is enough large. The station can be only powered by the co-located renewable and then the competitive ratio will become unchanged thereafter.

Fig. 2(e) shows how the competitive ratio varies with the transformer capacity. One observation is that the competitive ratio rises, as the transformer capacity increases. As mentioned above, the base load's uncertainty affects the algorithm's performance through the power drawn from the grid. Further, with larger transformer capacity, the charging station can draw more power from the grid. Thus, the uncertainty's impact on the performance increases and the competitive ratio goes up. Second, as the transformer capacity decreases, the decreasing rate of the competitive ratio also declines. When the transformer capacity is enough small, the power grid will have no power left for the charging station and thus gives no impact on the performance. At this time, only renewable generation impacts and the competitive ratio will not change any more.

Fig. 2(f) plots how the competitive ratio varies renewable generation. One observation is that the competitive ratio increases, as renewable generation grows. Different with the base load, the uncertainty of renewable generation affects the algorithm's performance directly. Thus, larger scale of renewable generation comes with higher impact on the performance and larger competitive ratios. Second, as renewable generation decreases, the decreasing rate of the competitive ratio also goes down. When renewable generation is enough small, e.g., when it equals zero, only the power grid affects the algorithm's performance. At this time, the performance is only affected by the base load (through the power grid). Note that the observations for Fig. 2(f) are true when renewable generation is less than some value. At the extreme case when renewable generation becomes enough large, all prediction errors can be then counteracted by renewable generation. One example of this case is when there is much surplus renewable generation, i.e., when the most conservative prediction is much larger than how much power all EVs need. At this time, all EVs will be charged at their maximum rates and the transformer works under its capacity limit. Thus, the proposed algorithm performs as well as the optimal algorithm.

2) *Charging Demand Balancing*: Fig. 3(a) illustrates the performance of the proposed charging demand balancing algorithm. The figure depicts how the competitive ratio η_u varies with all the three kinds of prediction errors. First, the competitive ratio rises as the inaccuracies of arrival demand prediction

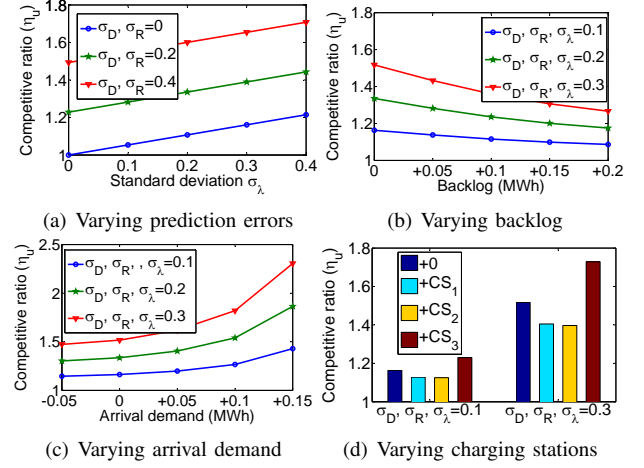


Fig. 3. Comparison on competitive ratios with varying prediction errors, backlog, arrival demand, and the number of charging stations.

(i.e., λ) increases. And, comparing three curves along y-axis, we can see that the competitive ratio also increases as the inaccuracies of renewable generation prediction and base load (i.e., σ_R, σ_D) increases. Here σ_R (σ_D) represents renewable (base load) predictions for all three charging stations, i.e., $\sigma_R = \sigma_{R_1} = \sigma_{R_2} = \sigma_{R_3}$ ($\sigma_D = \sigma_{D_1} = \sigma_{D_2} = \sigma_{D_3}$). Further, the increasing rate is linear as to the prediction error σ_λ of the arrival demand. These two observations also validate Theorem 5. Second, the proposed algorithm gives rather good performance, when the prediction inaccuracy is acceptable. For instance, when the prediction errors are less than 20%, the competitive ratios are less than 1.4.

Another observation is made from seeing four figures together: Fig. 2(a), Fig. 2(b), Fig. 2(c) and Fig. 3(a). That is, the impact on the algorithm's performance is small if considering each individual uncertainty, but it is rather large if considering the aggregated uncertainty. For example, as to $\sigma_\lambda = 0.2$ in Fig. 3(a), the competitive ratio is 1.11 when $\sigma_R = \sigma_D = 0$; it is 1.34 when $\sigma_R = \sigma_D = 0.2$. As to $\sigma_{D_2} = 0.2$ in Fig. 2(b), the competitive ratio is 1.28 when $\sigma_{R_2} = 0$; it is 1.32 when $\sigma_{R_2} = 0.2$. This observation also demonstrates the importance and necessity of studying the aggregated uncertainty instead of addressing each one individually. The simulation results and sensitivity analysis about the base load and renewable generation here are similar to those in the previous subsection. Thus, we focus on discussing how the algorithm's performance is affected by the backlog, arrival demand and the number of charging stations in the rest of this subsection.

Fig. 3(b) plots how the competitive ratio varies with the backlog in charging stations. The x-axis denotes how much the backlog is increased in each station. For example, the data point "0" means using the default setting; the point "+0.05" means that each charging station's backlog increases by 0.05 MWh. Each curve is plotted with fixed prediction errors of all the three aspects. From the figure, we can see that as the backlog grows, the competitive ratio decreases and the decreasing rate also declines. The reason is as follows. When the backlog becomes larger, i.e., the demand queues in stations become longer, the charging prices will become

higher. And thus, the probability of EVs choosing charging stations declines and they serve less of the arrival charging demand. Hence, the impact of arrival demand on the performance becomes lower and the competitive ratio decreases accordingly. When the backlog is enough large, the charging price will be the maximum and the charging stations will serve none of the arrival demand. At this time, the algorithm's performance is only affected by the uncertainties of base load and renewable and not by that of the arrival demand, and thus the competitive ratio will keep unchanged thereafter.

Fig. 3(c) demonstrates how the competitive ratio varies with the arrival charging demand. Similarly, the x-axis denotes how much the arrival demand is changed in each charging station as to the default setting. One observation here is that the competitive ratio increases as the arrival demand goes up. The reason is that the uncertainty of arrival demand directly affects the algorithm's performance and larger scale of arrival demand has higher impact on the performance. Second, as the arrival demand decreases, the decreasing rate of the competitive ratio also goes down. When the arrival demand is enough small, e.g., when it equals zero, only the base load and renewable generation give impact on the algorithm's performance. At this time, the arrival demand gives no impact on the performance and thus the competitive ratio will not change any more.

The final sensitivity analysis is about how the competitive ratio varies with the number of charging stations. Fig. 3(d) shows the result when the charging system has four charging stations. The legend describes which charging station is added to the default setting. For example, "+0" means using the default setting; "+ CS_1 " means adding one more station CS_1 to the default setting (thus two CS_1 in the new setting). From the figure, we can see that adding different charging station derives different variance in the competitive ratio. Adding station CS_1 or CS_2 reduces the competitive ratio while adding station CS_3 increases the ratio. Thus, one observation is that the number of charging stations has no direct impact on the algorithm's performance. This fact can be seen as an advantage of the proposed algorithm, which is, its performance suffers from no stability issue as to the scale of the charging system.

V. RELATED WORK

There are many existing works addressing different dimensions of electric vehicle charging. In this paper, we investigate two mostly closed related research threads: charging rate control and charging demand balancing.

Charging rate control. Ardakanian et al. [8] present a distributed control algorithm that fairly assigns charging rates to EVs while guaranteeing efficient usage of power network resources. Gan et al. [9] propose an optimal rate control algorithm that exploits the elasticity of EV loads to fill the valleys in power load profiles. Rahbari-Asr et al. [10] present a distributed power allocation algorithm that optimizes EV user satisfaction related to charging time and cost. Zheng et al. [11] discuss an on-line EV charging algorithm that optimizes the total value of served vehicles minus the energy cost. Kong et al. [17] studies deadline-aware rate control in the context of

demand response. Kong et al. [12] employ the event-driven model and borrow real-time scheduling theories to schedule EV charging loads for park-and-charge. Similarly, Yorie et al. [41] also borrows an algorithm from real-time scheduling, which is the least-laxity-first algorithm that first charges the most urgent vehicles.

Charging demand balancing. Ban et al. [13] formulate an EV allocation problem that addresses assigning EVs to multiple charging stations in order to minimize the waiting time of EV users. Qin et al. [15] present theoretical analysis to bound the waiting time of EV users through intelligently scheduling charging demand spatially and temporally. Liang et al. [14] leverage queueing network analysis to estimate charging demand for multiple charging stations. Hausler et al. [42] presents an approach that balances vehicles using a stochastic communication between EVs and charging stations. Bayram et al. [43] discuss a game theoretic framework in which vehicle routing and load balancing are induced through a pricing mechanism.

These above works study either charging rate control or demand balancing. This partial focus can cause the degradation to the stability of the power grid or QoS of EV customers. Kong et al. [16] try to solve this by considering both charging rate control and demand balancing together. However, the authors simply overlook the coupling relation between the two operations. More discussions about existing EV charging works can be found in survey papers such as [18], [44]. Different with all of the above works, this paper jointly manages charging rate control and demand balancing and carefully investigates the aggregated uncertainty caused by the coupling relation of the two operations.

VI. CONCLUSION

This paper presents an operational scheme that satisfies both the stability of the power grid and QoS to EV users. This operational scheme has a hierarchical structure, where the lower level performs charging rate control and the upper level carries out charging demand balancing. We propose stochastic optimization based algorithms for the two operations to handle the aggregated uncertainty caused by their coupling relation. These algorithms have provable robust performance guarantees that are independent on the distribution of prediction errors. The simulation results demonstrate the efficacy and also validate the theoretical results of the proposed algorithms.

ACKNOWLEDGMENT

This work was supported in part by NSF CNS-1505799, the Intel-NSF Partnership for Cyber-Physical Systems Security and Privacy, the NSERC Discovery Grant 341823, Canada Foundation for Innovation (CFI)'s John R. Evans Leaders Fund 23090, and McGill Tomlinson Scientist Award.

REFERENCES

- [1] Monthly Plug-In Sales Scorecard, <https://insideevs.com/monthly-plug-in-sales-scorecard/>, Jun., 2017, [Online accessed].
- [2] Navigant Research, "Electric vehicle market forecasts," <http://www.navigantresearch.com/>, Jun., 2017, [Online accessed].
- [3] ChargePoint, "We are ChargePoint," <http://www.chargepoint.com>, Jun., 2017, [Online accessed].

- [4] K. Clement-Nyns, E. Haesen, and J. Driesen, "The impact of charging plug-in hybrid electric vehicles on a residential distribution grid," *IEEE Trans. on Power Systems*, 2010.
- [5] J. Huang, V. Gupta, and Y.-F. Huang, "Scheduling algorithms for PHEV charging in shared parking lots," in *ACC*. IEEE, 2012.
- [6] S. Chen, Y. Ji, and L. Tong, "Large scale charging of electric vehicles," in *PES General Meeting*. IEEE, 2012.
- [7] J. Timpner and L. Wolf, "Design and evaluation of charging station scheduling strategies for electric vehicles," *IEEE Trans. on Intelligent Transportation Systems*, 2014.
- [8] O. Ardakanian, C. Rosenberg, and S. Keshav, "Distributed control of electric vehicle charging," in *ACM e-Energy*. ACM, 2013.
- [9] L. Gan, U. Topcu, and S. Low, "Optimal decentralized protocol for electric vehicle charging," *IEEE Trans. on Power Systems*, 2013.
- [10] N. Rahbari-Asr and M.-Y. Chow, "Cooperative distributed demand management for community charging of PHEV/PEVs based on KKT conditions and consensus networks," *IEEE Trans. on Industrial Informatics*, 2014.
- [11] Z. Zheng and N. B. Shroff, "Online welfare maximization for electric vehicle charging with electricity cost," in *ACM e-Energy*. ACM, 2014.
- [12] F. Kong, Q. Xiang, L. Kong, and X. Liu, "On-line event-driven scheduling for electric vehicle charging via park-and-charge," in *RTSS*. IEEE, 2016.
- [13] D. Ban, G. Michailidis, and M. Devetsikiotis, "Demand response control for PHEV charging stations by dynamic price adjustments," in *ISGT*. IEEE, 2012.
- [14] H. Liang, I. Sharma, W. Zhuang, and K. Bhattacharya, "Plug-in electric vehicle charging demand estimation based on queueing network analysis," in *PES General Meeting*. IEEE, 2014.
- [15] H. Qin and W. Zhang, "Charging scheduling with minimal waiting in a network of electric vehicles and charging stations," in *VANET*. ACM, 2011.
- [16] F. Kong, X. Liu, Z. Sun, and Q. Wang, "Smart rate control and demand balancing for electric vehicle charging," in *ICCPs*. IEEE, 2016.
- [17] F. Kong and X. Liu, "Distributed deadline and renewable aware electric vehicle demand response in the smart grid," in *RTSS*. IEEE, 2015.
- [18] L. Liu, F. Kong, X. Liu, Y. Peng, and Q. Wang, "A review on electric vehicles interacting with renewable energy in smart grid," *Renewable and Sustainable Energy Reviews*, 2015.
- [19] TimberRock Energy Solutions, <http://timberrockes.com/technology.html>, Jun., 2017, [Online accessed].
- [20] L. Gan, U. Topcu, and S. H. Low, "Stochastic distributed protocol for electric vehicle charging with discrete charging rate," in *PES General Meeting*. IEEE, 2012.
- [21] L. Chen, N. Li, S. Low, and J. Doyle, "Two market models for demand response in power networks," in *SmartGridComm*. IEEE, 2010.
- [22] L. Gkatzikis, I. Koutsopoulos, and T. Salonidis, "The role of aggregators in smart grid demand response markets," *IEEE Journal on Selected Areas in Communications*, 2013.
- [23] Z. Liu, I. Liu, S. Low, and A. Wierman, "Pricing data center demand response," in *SIGMETRICS*. ACM, 2014.
- [24] F. Kong, C. Dong, X. Liu, and H. Zeng, "Blowing hard is not all we want: Quantity vs quality of wind power in the smart grid," in *INFOCOM*. IEEE, 2014.
- [25] Z. Liu, A. Wierman, Y. Chen, B. Razon, and N. Chen, "Data center demand response: Avoiding the coincident peak via workload shifting and local generation," *Performance Evaluation*, 2013.
- [26] L. Gan, A. Wierman, U. Topcu, N. Chen, and S. H. Low, "Real-time deferrable load control: handling the uncertainties of renewable generation," in *ACM e-Energy*. ACM, 2013.
- [27] I. Moghram and S. Rahman, "Analysis and evaluation of five short-term load forecasting techniques," *IEEE Trans. on Power Systems*, 1989.
- [28] Wikipedia, "Charging station," https://en.wikipedia.org/wiki/Charging_station, Jun., 2017, [Online accessed].
- [29] B. Allaz and J.-L. Vila, "Cournot competition, forward markets and efficiency," *Journal of Economic theory*, 1993.
- [30] J. Yao, S. S. Oren, and I. Adler, "Two-settlement electricity markets with price caps and Cournot generation firms," *European Journal of Operational Research*, 2007.
- [31] J. Perez, "Fundamental principles of transformer thermal loading and protection," in *Annual Conference for Protective Relay Engineers*. IEEE, 2010.
- [32] G. Swift, S. Zocholl, M. Bajpai, J. Burger, C. Castro, S. Chano, F. Cobelo, P. De Sa, E. Fennell, J. Gilbert *et al.*, "Adaptive transformer thermal overload protection," *IEEE Trans. on Power Delivery*, 2001.
- [33] N. Hatzigiorgiou, H. Asano, R. Irvani, and C. Marnay, "Microgrids," *IEEE Power and Energy Magazine*, 2007.
- [34] F. Katiraei, R. Irvani, N. Hatzigiorgiou, and A. Dimeas, "Microgrids management," *IEEE Power and Energy Magazine*, 2008.
- [35] S. Boyd and L. Vandenberghe, *Convex optimization*. Cambridge university press, 2004.
- [36] M. J. Neely, "Stochastic network optimization with application to communication and queueing systems," *Synthesis Lectures on Communication Networks*, 2010.
- [37] C. Jin, X. Sheng, and P. Ghosh, "Energy efficient algorithms for electric vehicle charging with intermittent renewable energy sources," in *PES General Meeting*. IEEE, 2013.
- [38] Y. Cao, S. Tang, C. Li, P. Zhang, Y. Tan, Z. Zhang, and J. Li, "An optimized EV charging model considering TOU price and SOC curve," *IEEE Trans. on Smart Grid*, 2012.
- [39] R. S. Winer, "A reference price model of brand choice for frequently purchased products," *Journal of consumer research*, 1986.
- [40] Federal Energy Regulatory Commission, "Electric power markets," <http://www.ferc.gov/market-oversight/mkt-electric/overview.asp>, Jun., 2017, [Online accessed].
- [41] Y. Nakahira, N. Chen, L. Chen, and S. H. Low, "Smoothed least-laxity-first algorithm for ev charging," in *ACM e-Energy*. ACM, 2017.
- [42] F. Hausler, E. Crisostomi, A. Schlote, I. Radosch, and R. Shorten, "Stochastic park-and-charge balancing for fully electric and plug-in hybrid vehicles," *IEEE Trans. on Intelligent Transportation Systems*, 2014.
- [43] I. S. Bayram, G. Michailidis, and M. Devetsikiotis, "Unsplittable load balancing in a network of charging stations under qos guarantees," *IEEE Transactions on Smart Grid*, 2015.
- [44] Q. Wang, X. Liu, J. Du, and F. Kong, "Smart charging for electric vehicles: A survey from the algorithmic perspective," *IEEE Communications Surveys & Tutorials*, 2016.

APPENDIX

Proof for Lemma 2. Given $R = (1 + \varepsilon_r)\tilde{R}$ and $D = (1 + \varepsilon_d)\tilde{D}$, we have the following deduction. Let $\varepsilon_k^+ = \Psi_k(\varepsilon_d^+\tilde{D} - \varepsilon_r^+\tilde{R})$ and $\varepsilon_k^- = \Psi_k(\varepsilon_d^-\tilde{D} - \varepsilon_r^-\tilde{R})$, where $a^+ = \max\{0, a\}$ and $a^- = \min\{0, a\}$.

$$\begin{aligned}
\tilde{p}_k &= [\bar{P}_k - \tilde{\beta}_k]_0^{\bar{P}_k} = [\bar{P}_k - \tilde{\beta}_k]^{\bar{P}_k} - [\bar{P}_k - \tilde{\beta}_k]_0^0 \\
&= \left([\bar{P}_k - \tilde{\beta}_k - \varepsilon_k]^{\bar{P}_k} + [\varepsilon_k + \tilde{\beta}_k]_0^{\varepsilon_k^+} + [-\tilde{\beta}_k]_{\varepsilon_k^-}^0 \right) - \\
&\quad \left([\bar{P}_k - \tilde{\beta}_k - \varepsilon_k]_0^0 + [\bar{P}_k - \tilde{\beta}_k]_{\varepsilon_k^-}^0 + [\varepsilon_k - \bar{P}_k + \tilde{\beta}_k]_0^{\varepsilon_k^+} \right) \\
&= [\bar{P}_k - \tilde{\beta}_k - \varepsilon_k]^{\bar{P}_k} - [\bar{P}_k - \tilde{\beta}_k - \varepsilon_k]_0^0 + \varphi_k^+ + \varphi_k^- \\
&= \hat{p}_k + \varphi_k.
\end{aligned}$$

Proof for Lemma 3. (i) Proof for the expectations. Since $\varepsilon_r = \varepsilon_r^+ + \varepsilon_r^-$, we have $\mathbb{E}[\varepsilon_r] = \mathbb{E}[\varepsilon_r^+ + \varepsilon_r^-] = 0$, and thus $\mathbb{E}[\varepsilon_r^+] = -\mathbb{E}[\varepsilon_r^-]$. Then, it follows that

$$\begin{aligned}
\sigma_r^2 &= \mathbb{E}[\varepsilon_r^2] = \mathbb{E}[(\varepsilon_r^+ + \varepsilon_r^-)^2] \\
&= \mathbb{E}[(\varepsilon_r^+)^2] + \mathbb{E}[(\varepsilon_r^-)^2] + 2\mathbb{E}[\varepsilon_r^+ \varepsilon_r^-] \\
&= \mathbb{E}[(\varepsilon_r^+)^2] + \mathbb{E}[(\varepsilon_r^-)^2] \\
&\geq \frac{\mathbb{E}[\varepsilon_r^+]^2}{\mathbb{P}(\varepsilon_r \geq 0)} + \frac{\mathbb{E}[\varepsilon_r^-]^2}{\mathbb{P}(\varepsilon_r < 0)} \\
&= \mathbb{E}[\varepsilon_r^+]^2 \left(\frac{1}{\mathbb{P}(\varepsilon_r \geq 0)} + \frac{1}{1 - \mathbb{P}(\varepsilon_r \geq 0)} \right) \\
&= \mathbb{E}[\varepsilon_r^+]^2 \left(\frac{1}{\mathbb{P}(\varepsilon_r \geq 0)(1 - \mathbb{P}(\varepsilon_r \geq 0))} \right) \\
&\geq 4\mathbb{E}[\varepsilon_r^+]^2, \{ \cdot : \text{equality attains when } \mathbb{P}(\varepsilon_r \geq 0) = \frac{1}{2} \}
\end{aligned} \tag{29}$$

where $\mathbb{P}(\cdot)$ is the probability density function. Rearranging the inequality, we have $\mathbb{E}[\epsilon_r^+] \leq \frac{\sigma_r}{2}$ and thus $\mathbb{E}[\epsilon_r^-] \geq -\frac{\sigma_r}{2}$. Hence, it follows that $\mathbb{E}[\epsilon_r^+ - \epsilon_r^-] \leq \sigma_r$. The inequality of Eqn. (29) holds because

$$\begin{aligned} \mathbb{E}[(\epsilon_r^+)^2] \mathbb{P}(\epsilon_r \geq 0) &= \int_0^\infty h^2 d\mathbb{F}_{\epsilon_r}(h) \int_0^\infty 1 d\mathbb{F}_{\epsilon_r}(h) \\ &\geq \left(\int_0^\infty h d\mathbb{F}_{\epsilon_r}(h) \right)^2 = \mathbb{E}[(\epsilon_r^+)]^2, \end{aligned}$$

where $\mathbb{F}_{\epsilon_r}(\cdot)$ is the cumulative distribution function. Rearranging the inequality, we have $\mathbb{E}[(\epsilon_r^+)^2] \geq \frac{\mathbb{E}[\epsilon_r^+]^2}{\mathbb{P}(\epsilon_r \geq 0)}$. Using similar deduction we can also have $\mathbb{E}[(\epsilon_r^-)^2] \geq \frac{\mathbb{E}[\epsilon_r^-]^2}{\mathbb{P}(\epsilon_r < 0)}$. Similar proving process can be applied to the prediction error ϵ_d and we have $\mathbb{E}[\epsilon_d^+ - \epsilon_d^-] \leq \sigma_d$. This proof is similar to that in [25].

(ii) Proof for the variances. We have the deduction:

$$\begin{aligned} \mathbb{V}(\epsilon_r^+ - \epsilon_r^-) &= \mathbb{V}(\epsilon_r^+) + \mathbb{V}(\epsilon_r^-) - 2(\mathbb{E}[\epsilon_r^+ \epsilon_r^-] - \mathbb{E}[\epsilon_r^+] \mathbb{E}[\epsilon_r^-]) \\ &= \mathbb{V}(\epsilon_r^+) + \mathbb{V}(\epsilon_r^-) - 2\mathbb{E}[\epsilon_r^+] \mathbb{E}[\epsilon_r^-] + 4\mathbb{E}[\epsilon_r^+] \mathbb{E}[\epsilon_r^-] \\ &= \mathbb{V}(\epsilon_r^+ + \epsilon_r^-) + 4\mathbb{E}[\epsilon_r^+] \mathbb{E}[\epsilon_r^-] \\ &\leq \mathbb{V}(\epsilon_r) = \sigma_r^2. \end{aligned}$$

Similar proving process can be applied to the prediction error ϵ_d and thus we have $\mathbb{V}(\epsilon_d^+ - \epsilon_d^-) \leq \sigma_d^2$. We have finished the proof of this lemma.

Proof for Theorem 4. Plugging the solution $\tilde{\mathbf{p}}$ of problem \mathbf{P}_1^e and solution $\hat{\mathbf{p}}$ of problem \mathbf{P}_1^o into Eqn. (7), replacing \tilde{p}_k with $\hat{p}_k + \varphi_k$, and using Lemma 2, we have Eqn. (30).

$$\begin{aligned} \eta_l &= \frac{\mathbb{E}[u(\tilde{\mathbf{p}})]}{\mathbb{E}[u(\hat{\mathbf{p}})]} = \frac{\mathbb{E}\left[\frac{1}{2} \sum_k \alpha_k (\bar{P}_k - \tilde{p}_k)^2 + \frac{1}{2} (\sum_k \tilde{p}_k + D - R - L)^+\right]}{\mathbb{E}[u(\hat{\mathbf{p}})]} \\ &= \frac{\mathbb{E}[u(\tilde{\mathbf{p}})]}{\mathbb{E}[u(\hat{\mathbf{p}})]} \mathbb{E}\left[\frac{1}{2} \sum_k \alpha_k (\bar{P}_k - \hat{p}_k - \varphi_k)^2 + \frac{1}{2} (\sum_k \hat{p}_k + \sum_k \varphi_k + D - R - L)^+\right] \{\cdot: Lemma 2\} \\ &\leq 1 + \frac{1}{\mathbb{E}[u(\hat{\mathbf{p}})]} \mathbb{E}\left[\frac{1}{2} \sum_k \alpha_k \varphi_k^2 - \sum_k \alpha_k (\bar{P}_k - \hat{p}_k) \varphi_k + \frac{1}{2} (\sum_k \varphi_k)^+ + \hat{e} \sum_k \varphi_k^+\right] \\ &\leq 1 + \frac{1}{\mathbb{E}[u(\hat{\mathbf{p}})]} \left(\underbrace{\frac{1}{2} \mathbb{E} \left[\sum_k \alpha_k \varphi_k^2 \right]}_{Y_1} + \underbrace{\left(-\mathbb{E} \left[\sum_k \alpha_k (\bar{P}_k - \hat{p}_k) \varphi_k \right] \right)}_{Y_2} \right. \\ &\quad \left. + \frac{1}{2} \mathbb{E} \left[\left(\sum_k \varphi_k^+ \right)^2 \right] + \hat{e} \mathbb{E} \left[\sum_k \varphi_k^+ \right] \right) \quad (30) \end{aligned}$$

Then, to bound the competitive ratio, we only need to bound the four items from Y_1 to Y_4 respectively. The corresponding deduction for bounding the four items is as follows.

(i) Bounding item Y_1 .

$$\begin{aligned} Y_1 &= \frac{1}{2} \mathbb{E} \left[\sum_k \alpha_k (\varphi_k^+ + \varphi_k^-)^2 \right] \\ &\leq \frac{1}{2} \sum_k \alpha_k \mathbb{E} \left[(\epsilon_k^+ - \epsilon_k^-)^2 \right] \\ &= \frac{1}{2} \sum_k \alpha_k \left(\mathbb{V}(\epsilon_k^+ - \epsilon_k^-) + (\mathbb{E}[\epsilon_k^+ - \epsilon_k^-])^2 \right) \end{aligned}$$

$$\begin{aligned} &\leq \frac{1}{2} \sum_k \alpha_k \left(\Psi_k^2 \left(\tilde{D}^2 \mathbb{V}(\epsilon_d^+ - \epsilon_d^-) + \tilde{R}^2 \mathbb{V}(\epsilon_r^+ - \epsilon_r^-) \right) \right. \\ &\quad \left. + \Psi_k^2 \left(\tilde{R} \mathbb{E}[\epsilon_r^+ - \epsilon_r^-] + \tilde{D} \mathbb{E}[\epsilon_d^+ - \epsilon_d^-] \right)^2 \right) \{\cdot: Lemma 2\} \\ &\leq \frac{1}{2} \sum_k \alpha_k \left(\Psi_k^2 \left(\tilde{D}^2 \sigma_d^2 + \tilde{R}^2 \sigma_r^2 \right) + \Psi_k^2 \left(\tilde{D} \sigma_d + \tilde{R} \sigma_r \right)^2 \right) \{\cdot: Lemma 3\} \\ &= \left(\tilde{D}^2 \sigma_d^2 + \tilde{R}^2 \sigma_r^2 + \tilde{D} \sigma_d \tilde{R} \sigma_r \right) \sum_k \alpha_k \Psi_k^2. \end{aligned}$$

(ii) Bounding item Y_2 .

$$\begin{aligned} Y_2 &= -\sum_k \alpha_k (\bar{P}_k - \hat{p}_k) \mathbb{E}[\varphi_k^+ + \varphi_k^-] \\ &\leq \sum_k \alpha_k (\bar{P}_k - \hat{p}_k) \mathbb{E}[\epsilon_k^+ - \epsilon_k^-] \\ &\leq \sum_k \alpha_k (\bar{P}_k - \hat{p}_k) \Psi_k \left(\tilde{R} \mathbb{E}[\epsilon_r^+ - \epsilon_r^-] + \tilde{D} \mathbb{E}[\epsilon_d^+ - \epsilon_d^-] \right) \{\cdot: Lemma 2\} \\ &\leq \left(\tilde{D} \sigma_d + \tilde{R} \sigma_r \right) \sum_k \alpha_k (\bar{P}_k - \hat{p}_k) \Psi_k \{\cdot: Lemma 3\}. \end{aligned}$$

(iii) Bounding item Y_3 .

$$\begin{aligned} Y_3 &= \frac{1}{2} \left(\mathbb{V}(\sum_k (\epsilon_k^+ - \epsilon_k^-)) + (\mathbb{E}[\epsilon_k^+ - \epsilon_k^-])^2 \right) \\ &\leq \frac{1}{2} \left((\sum_k \Psi_k)^2 \mathbb{V}(\epsilon_r^+ \tilde{R} - \epsilon_r^- \tilde{R} + \epsilon_d^+ \tilde{D} - \epsilon_d^- \tilde{D}) \right. \\ &\quad \left. + (\sum_k \Psi_k)^2 \left(\tilde{R} \mathbb{E}[\epsilon_r^+ - \epsilon_r^-] + \tilde{D} \mathbb{E}[\epsilon_d^+ - \epsilon_d^-] \right)^2 \right) \{\cdot: Lemma 2\} \\ &\leq \frac{1}{2} \left((\sum_k \Psi_k)^2 \left(\tilde{R}^2 \mathbb{V}(\epsilon_r^+ - \epsilon_r^-) + \tilde{D}^2 \mathbb{V}(\epsilon_d^+ - \epsilon_d^-) \right) \right. \\ &\quad \left. + (\sum_k \Psi_k)^2 \left(\tilde{R} \mathbb{E}[\epsilon_r^+ - \epsilon_r^-] + \tilde{D} \mathbb{E}[\epsilon_d^+ - \epsilon_d^-] \right)^2 \right) \quad (31) \\ &\leq \left(\tilde{D}^2 \sigma_d^2 + \tilde{R}^2 \sigma_r^2 + \tilde{D} \sigma_d \tilde{R} \sigma_r \right) (\sum_k \Psi_k)^2 \{\cdot: Lemma 3\}. \end{aligned}$$

Eqn. (31) holds because $\text{COV}(\epsilon_r^+ - \epsilon_r^-, \epsilon_d^+ - \epsilon_d^-) = 0$, where $\text{COV}(\cdot, \cdot)$ is the covariance. This follows since ϵ_r^+ or ϵ_r^- is independent of ϵ_d^+ or ϵ_d^- , and the covariance between each pair of them is zero. The deduction is as follows:

$$\begin{aligned} &\text{COV}(\epsilon_r^+ - \epsilon_r^-, \epsilon_d^+ - \epsilon_d^-) \\ &= \text{COV}(\epsilon_r^+, \epsilon_d^+) - \text{COV}(\epsilon_r^+, \epsilon_d^-) - \text{COV}(\epsilon_r^-, \epsilon_d^+) + \text{COV}(\epsilon_r^-, \epsilon_d^-) = 0. \end{aligned}$$

(iv) Bounding item Y_4 .

$$\begin{aligned} Y_4 &= \hat{e} \mathbb{E} \left[\sum_k \varphi_k^+ \right] \\ &\leq \hat{e} \left(\sum_k \Psi_k \mathbb{E} \left[\epsilon_r^+ \tilde{R} - \epsilon_r^- \tilde{R} + \epsilon_d^+ \tilde{D} - \epsilon_d^- \tilde{D} \right] \right) \{\cdot: Lemma 2\} \\ &\leq \hat{e} \left(\tilde{D} \sigma_d + \tilde{R} \sigma_r \right) (\sum_k \Psi_k) \{\cdot: Lemma 3\}. \end{aligned}$$

Combining the four items into Eqn. (30), we have the bound of the competitive ratio, which is right the one stated in the theorem. We thus complete the proof.

Proof for Theorem 5. To obtain the competitive ratio, we first bound the difference between $\mathbb{E}[c(\tilde{\mathbf{q}})]$ and $\mathbb{E}[c(\hat{\mathbf{q}})]$, as shown in Eqn. (32).

$$\begin{aligned} &\mathbb{E}[c(\tilde{\mathbf{q}})] - \mathbb{E}[c(\hat{\mathbf{q}})] \\ &= \sum_i \left(\underbrace{\mathbb{E} \left[\frac{\lambda \tilde{q}}{\Delta q} (\hat{\theta}_i - \tilde{\theta}_i) \right]}_{Z_1} + \underbrace{\mathbb{E} \left[\frac{2\omega \lambda}{\Delta q} \left([Q_i - \hat{\mu}_i]^+ \hat{\theta}_i - [Q_i - \tilde{\mu}_i]^+ \tilde{\theta}_i \right) \right]}_{Z_2} \right) \\ &\quad + \underbrace{\mathbb{E} \left[\frac{\lambda}{\Delta q} \left(1 - \frac{\omega \lambda}{\Delta q} \right) (\hat{\theta}_i^2 - \tilde{\theta}_i^2) \right]}_{Z_3} + \underbrace{\mathbb{E} \left[\omega \left(([Q_i - \tilde{\mu}_i]^+)^2 - ([Q_i - \hat{\mu}_i]^+)^2 \right) \right]}_{Z_4} \quad (32) \end{aligned}$$

To bound this difference, we only need to bound the four items from Z_1 to Z_4 respectively. The corresponding deduction is as follows.

(i) Bounding item Z_1 .

$$\begin{aligned}
Z_1 &= \frac{\lambda \bar{q}}{\Delta q} \mathbb{E} \left[\hat{\theta}_i - \tilde{\theta}_i \right] \\
&= \lambda \bar{q} \mathbb{E} \left[\frac{\omega [Q_i - \hat{\mu}_i - \sum_k \varphi_{i,k}^+]}{\Delta q - \omega \lambda} - \frac{\omega [Q_i - \hat{\mu}_i]^+}{\Delta q - \omega \lambda} + \frac{\bar{q}}{2\Delta q - 2\omega \lambda} - \frac{\bar{q}}{2\Delta q - 2\omega \lambda} \right] \\
\{&: \text{According to Lemma 2, } \tilde{\mu}_i - \hat{\mu}_i = \sum_k (\tilde{p}_{i,k} - \hat{p}_{i,k}) = \sum_k \varphi_{i,k}, \\
&\text{where index } i, k \text{ denotes EV}_k \text{ at charging station CS}_i\} \\
&\leq \lambda \bar{q} \mathbb{E} \left[\frac{\omega [Q_i - \hat{\mu}_i - \sum_k \varphi_{i,k}^-]}{\Delta q - \omega \lambda} - \frac{\omega [Q_i - \hat{\mu}_i]^+}{\Delta q - \omega \lambda} + \frac{\bar{q}}{2\Delta q - 2\omega \lambda} - \frac{\bar{q}}{2\Delta q - 2\omega \lambda} \right] \\
&= \lambda \bar{q} \mathbb{E} \left[\frac{\omega [Q_i - \hat{\mu}_i]^+}{\Delta q - \omega \lambda} + \frac{\omega (-\sum_k \varphi_{i,k}^-)}{\Delta q - \omega \lambda} - \frac{\omega [Q_i - \hat{\mu}_i]^+}{\Delta q - \omega \lambda} + \frac{\bar{q}}{2\Delta q - 2\omega \lambda} - \frac{\bar{q}}{2\Delta q - 2\omega \lambda} \right] \\
&= \lambda \bar{q} \mathbb{E} \left[\frac{\frac{\bar{q}}{2} + \omega [Q_i - \hat{\mu}_i]^+}{\Delta q - \omega \lambda} \left(\frac{\Delta q - \omega \tilde{\lambda}(1 + \varepsilon_\lambda)}{\Delta q - \omega \lambda} - 1 \right) - \frac{\omega (\sum_k \varphi_{i,k}^-)}{\Delta q - \omega \lambda} \right] \\
&\leq \frac{\omega \bar{q} \lambda \tilde{\lambda} (\frac{\bar{q}}{2} + \omega [Q_i - \hat{\mu}_i]^+)}{(\Delta q - \omega \lambda)(\Delta q - \omega \lambda)} \mathbb{E} [-\varepsilon_\lambda^-] + \frac{\omega \lambda \bar{q}}{\Delta q - \omega \lambda} \mathbb{E} [-\sum_k \varphi_{i,k}^-] \\
&\leq \frac{\omega \bar{q} \lambda \tilde{\lambda} (\frac{\bar{q}}{2} + \omega [Q_i - \hat{\mu}_i]^+)}{2(\Delta q - \omega \lambda)(\Delta q - \omega \lambda)} \sigma_\lambda + \frac{\omega \lambda \bar{q}}{\Delta q - \omega \lambda} (\tilde{D}_i \sigma_d + \tilde{R}_i \sigma_r) (\sum_k \Psi_{i,k}) \quad (33)
\end{aligned}$$

The last inequality of Eqn. (33) attains due to the following fact. First, using a similar proof as in Lemma 3, we can have $\mathbb{E} [-\varepsilon_\lambda^-] \geq -\frac{\sigma_\lambda}{2}$ and thus $\mathbb{E} [-\varepsilon_\lambda^-] \leq \frac{\sigma_\lambda}{2}$. Thus, the first item of Eqn. (33) holds. Second, the second item of Eqn. (33) attains due to the following fact.

$$\begin{aligned}
\mathbb{E} [-\sum_k \varphi_{i,k}^-] &\leq \mathbb{E} \left[\sum_k (\varepsilon_{i,k}^+ - \varepsilon_{i,k}^-) \right] \\
&\leq \sum_k \Psi_k \mathbb{E} \left[\varepsilon_r^+ \tilde{R}_i - \varepsilon_r^- \tilde{R}_i + \varepsilon_d^+ \tilde{D}_i - \varepsilon_d^- \tilde{D}_i \right] \{ : \text{Lemma 2} \} \\
&\leq (\tilde{D}_i \sigma_d + \tilde{R}_i \sigma_r) (\sum_k \Psi_{i,k}) \{ : \text{Lemma 3} \}. \quad (34)
\end{aligned}$$

(ii) Bounding item Z_2 .

$$\begin{aligned}
Z_2 &= \mathbb{E} \left[\frac{2\omega \lambda}{\Delta q} \left([Q_i - \hat{\mu}_i]^+ \hat{\theta}_i - [Q_i - \tilde{\mu}_i]^+ \tilde{\theta}_i \right) \right] \\
&\leq 2\omega \lambda \mathbb{E} \left[\frac{\omega ([Q_i - \hat{\mu}_i]^+ - \sum_k \varphi_{i,k}^-)}{\Delta q - \omega \lambda} - \frac{\omega ([Q_i - \hat{\mu}_i]^+)}{\Delta q - \omega \lambda} \right. \\
&\quad \left. + \frac{\bar{q} ([Q_i - \hat{\mu}_i]^+ - \sum_k \varphi_{i,k}^-)}{2\Delta q - 2\omega \lambda} - \frac{\bar{q} [Q_i - \hat{\mu}_i]^+}{2\Delta q - 2\omega \lambda} \right] \\
&= 2\omega \lambda \mathbb{E} \left[\frac{[Q_i - \hat{\mu}_i]^+ (\frac{\bar{q}}{2} + \omega [Q_i - \hat{\mu}_i])}{\Delta q - \omega \lambda} \left(\frac{\Delta q - \omega \tilde{\lambda}(1 + \varepsilon_\lambda)}{\Delta q - \omega \lambda} - 1 \right) \right. \\
&\quad \left. + \frac{(\frac{\bar{q}}{2} + 2\omega [Q_i - \hat{\mu}_i]^+)}{\Delta q - \omega \lambda} \left(-\sum_k \varphi_{i,k}^- \right) + \frac{\omega}{\Delta q - \omega \lambda} \left(\sum_k \varphi_{i,k}^- \right)^2 \right] \\
&\leq \frac{2\omega^2 \lambda \tilde{\lambda} [Q_i - \hat{\mu}_i]^+ (\frac{\bar{q}}{2} + \omega [Q_i - \hat{\mu}_i])}{(\Delta q - \omega \lambda)(\Delta q - \omega \lambda)} \mathbb{E} [-\varepsilon_\lambda^-] + \frac{2\omega^2 \lambda}{\Delta q - \omega \lambda} \mathbb{E} \left[\left(\sum_k \varphi_{i,k}^- \right)^2 \right] \\
&\quad + \frac{2\omega \lambda (\frac{\bar{q}}{2} + 2\omega [Q_i - \hat{\mu}_i]^+)}{\Delta q - \omega \lambda} \mathbb{E} [-\sum_k \varphi_{i,k}^-] \\
&\leq \frac{\omega^2 \lambda \tilde{\lambda} [Q_i - \hat{\mu}_i]^+ (\frac{\bar{q}}{2} + \omega [Q_i - \hat{\mu}_i])}{(\Delta q - \omega \lambda)(\Delta q - \omega \lambda)} \sigma_\lambda \quad (35) \\
&\quad + \frac{4\omega^2 \lambda}{\Delta q - \omega \lambda} (\sum_k \Psi_{i,k})^2 (\tilde{D}_i^2 \sigma_d^2 + \tilde{R}_i^2 \sigma_r^2 + \tilde{D}_i \sigma_d \tilde{R}_i \sigma_r) \quad (36) \\
&\quad + \frac{2\omega \lambda (\frac{\bar{q}}{2} + 2\omega [Q_i - \hat{\mu}_i]^+)}{\Delta q - \omega \lambda} (\sum_k \Psi_{i,k}) (\tilde{D}_i \sigma_d + \tilde{R}_i \sigma_r). \quad (37)
\end{aligned}$$

The item Eqn. (35) holds due to $\mathbb{E} [-\varepsilon_\lambda^-] \leq \frac{\sigma_\lambda}{2}$ (by a similar proof as in Lemma 3). The deduction for bounding $\mathbb{E} [(\sum_k \varphi_{i,k}^-)^2]$ is similar to that for bounding item Y_3 in Theorem 4. Thus, the item Eqn. (36) holds. The item Eqn. (37) attains because of the above deduction of Eqn. (34).

(iii) Bounding item Z_3 .

$$\begin{aligned}
Z_3 &= \mathbb{E} \left[\frac{\lambda}{\Delta q} \left(1 - \frac{\omega \lambda}{\Delta q} \right) (\hat{\theta}_i^2 - \tilde{\theta}_i^2) \right] \\
&\leq \lambda (\Delta q - \omega \lambda) \mathbb{E} \left[\left(\frac{2\omega [Q_i - \hat{\mu}_i]^+ + \bar{q}}{2\Delta q - 2\omega \lambda} \right)^2 - \left(\frac{2\omega [Q_i - \hat{\mu}_i - \sum_k \varphi_{i,k}^+] + \bar{q}}{2\Delta q - 2\omega \lambda} \right)^2 \right] \\
&= \lambda (\Delta q - \omega \lambda) \mathbb{E} \left[\left(\frac{2\omega [Q_i - \hat{\mu}_i]^+ + \bar{q}}{2\Delta q - 2\omega \lambda} \right)^2 - \left(\frac{2\omega [Q_i - \hat{\mu}_i]^+ + \bar{q} - 2\omega [Q_i - \hat{\mu}_i]_0 \sum_k \varphi_{i,k}^+}{2\Delta q - 2\omega \lambda} \right)^2 \right] \\
&\leq \frac{\lambda (\Delta q - \omega \lambda) (2\omega [Q_i - \hat{\mu}_i]^+ + \bar{q})^2}{(2\Delta q - 2\omega \lambda)^2 (\Delta q - \omega \lambda)^2} \mathbb{E} \left[(\Delta q - \omega \tilde{\lambda})^2 - (\Delta q - \omega \tilde{\lambda} (1 + \varepsilon_\lambda))^2 \right] \\
&\quad + \frac{\omega \lambda (\Delta q - \omega \lambda) (2\omega [Q_i - \hat{\mu}_i]^+ + \bar{q})}{(\Delta q - \omega \lambda)^2} \mathbb{E} [\sum_k \varphi_{i,k}^+] \\
&\leq \frac{\omega \lambda \tilde{\lambda} (2\Delta q - \omega (\lambda + \tilde{\lambda})) (2\omega [Q_i - \hat{\mu}_i]^+ + \bar{q})^2}{(\Delta q - \omega \lambda) (2\Delta q - 2\omega \tilde{\lambda})^2} \mathbb{E} [\varepsilon_\lambda^+] \\
&\quad + \frac{\omega \lambda (\Delta q - \omega \lambda) (2\omega [Q_i - \hat{\mu}_i]^+ + \bar{q})}{(\Delta q - \omega \lambda)^2} \mathbb{E} [\sum_k \varphi_{i,k}^+] \\
&\leq \frac{\omega \lambda \tilde{\lambda} (2\Delta q - \omega (\lambda + \tilde{\lambda})) (\frac{\bar{q}}{2} + \omega [Q_i - \hat{\mu}_i]^+)^2}{2(\Delta q - \omega \lambda) (\Delta q - \omega \tilde{\lambda})^2} \sigma_\lambda \\
&\quad + \frac{\omega \lambda (\Delta q - \omega \lambda) (2\omega [Q_i - \hat{\mu}_i]^+ + \bar{q})}{(\Delta q - \omega \tilde{\lambda})^2} (\sum_k \Psi_{i,k}) (\tilde{D}_i \sigma_d + \tilde{R}_i \sigma_r). \quad (38)
\end{aligned}$$

The last inequality of Eqn. (38) attains due to the following fact. First, using a similar proof as in Lemma 3, we can have $\mathbb{E} [\varepsilon_\lambda^+] \leq \frac{\sigma_\lambda}{2}$ and thus the first item of Eqn. (38) holds. Second, using a similar deduction of bounding item Y_4 in Theorem 4, we can have the correctness of its second item.

(iv) Bounding item Z_4 .

$$\begin{aligned}
Z_4 &= \mathbb{E} \left[\omega \left(([Q_i - \tilde{\mu}_i]^+)^2 - ([Q_i - \hat{\mu}_i]^+)^2 \right) \right] \\
&\leq \omega \mathbb{E} \left[\left([Q_i - \hat{\mu}_i - \sum_k \varphi_{i,k}^-]^+ \right)^2 - ([Q_i - \hat{\mu}_i]^+)^2 \right] \\
&\leq \omega \mathbb{E} \left[\left([Q_i - \hat{\mu}_i]^+ - \sum_k \varphi_{i,k}^- \right)^2 - ([Q_i - \hat{\mu}_i]^+)^2 \right] \\
&= \omega \mathbb{E} \left[\left(\sum_k \varphi_{i,k}^- \right)^2 + 2\omega [Q_i - \hat{\mu}_i]^+ \mathbb{E} [-\sum_k \varphi_{i,k}^-] \right] \\
&\leq 2\omega (\sum_k \Psi_{i,k})^2 (\tilde{D}_i^2 \sigma_d^2 + \tilde{R}_i^2 \sigma_r^2 + \tilde{D}_i \sigma_d \tilde{R}_i \sigma_r) \\
&\quad + 2\omega [Q_i - \hat{\mu}_i]^+ (\sum_k \Psi_{i,k}) (\tilde{D}_i \sigma_d + \tilde{R}_i \sigma_r). \quad (39)
\end{aligned}$$

The deduction for bounding $\mathbb{E} [(\sum_k \varphi_{i,k}^-)^2]$ is similar to that for bounding item Y_3 in Theorem 4. So the first item of Eqn. (39) holds. The second item of Eqn. (39) attains because of the above deduction of Eqn. (34).

We now complete bounding the four items in Eqn. (32). Combining them, we have the bound of the competitive ratio, which is right the one stated in the theorem. We thus complete the proof and the truth of the theorem follows.